35th Annual International Conference of the IEEE EMBS
Osaka, Japan, 3 - 7 July, 2013

Effects of Stenosis on the Porcine Left Anterior Descending Arterial Tree*

Liang Zhong, Boyang Su, Jun-Mei Zhang, Yunlong Huo, Hwa Liang Leo, Ghassan S. Kassab, Ru San Tan

Abstract—**In this study, hemodynamics in the normal and diseased left anterior descending (LAD) arterial trees were compared to estimate the effects of stenosis on the flow rate distribution, detailed flow field and wall shear stress (WSS) distributions on both transient and steady flow conditions. The anatomical model was reconstructed from computed tomography (CT) images of a normal porcine heart. Stenosis was imposed at the trunk of LAD tree with different area stenosis ratios (25%, 50%, 75% and 90%) to study the effect of stenosis. It has been found that the steady-state simulation is competent to demonstrate the prominent flow features of transit flow. Only significant stenosis altered the flow rate considerably, and its effects diminished at the downstream bifurcations. Based on the WSS distribution, non-significant stenosis potentially led to the development of atherosclerosis near the ostium of the downstream side branch and significant stenosis might promote atherosclerosis in its wake.**

I. INTRODUCTION

Coronary artery disease (CHD) is one of the leading causes of death worldwide. It is usually resulted from atherosclerosis, which is caused by the formation of plaques on the arterial wall. The growth of plaques leads to arterial stenosis, which can cause further platelet activation and even coronary occlusion.

*Research supported by National Medical Research Council (NMRC/EDG/1037/2011) and SingHealth (SHF/FG503P/2012).

Liang Zhong is with the Cardiac Mechanics Engineering and Physiology Unit, National Heart Center, Singapore, Mistri Wing 17, 3rd Hospital Avenue, 168752, Singapore (corresponding author, phone: (65) - 64367684; e-mail: zhong.liang@nhcs.com.sg).

Boyang Su is with Biofluid Mechanics Research Laboratory, Block E3, #05-18A, 2 Engineering Drive 3, Department of Bioengineering, National University of Singapore, Singapore 117576 (e-mail: biesub@nus.edu.sg).

Jun-Mei Zhang is with the Cardiac Mechanics Engineering and Physiology Unit, National Heart Center, Singapore, Mistri Wing 17, 3rd Hospital Avenue, 168752, Singapore (e-mail: zhang.junmei@nhcs.com.sg; zhangjunmei@gmail.com).

Yunlong Huo is with the Department of Mechanics and Engineering Science, College of Engineering, Peking University, Beijing, 100871, China (e-mail: yhuo@pku.edu.cn)

Hwa Liang Leo is with Department of Bioengineering, Block EA, #03-12, 9 Engineering Drive 1, National University of Singapore, Singapore 117576 (e-mail: bielhl@nus.edu.sg)

Ghassan S. Kassab is with the Departments of Biomedical Engineering, Surgery, and Cellular and Integrative Physiology, Indiana University Purdue University Indianapolis, Indianapolis, IN 46202, USA (e-mail: gkassab@3dtholdings.com).

Ru San Tan is with the Cardiac Mechanics Engineering and Physiology Unit, National Heart Center, Singapore, Mistri Wing 17, 3rd Hospital Avenue, 168752, Singapore (e-mail: tan.ru.san@nhcs.com.sg).

Computational fluid dynamics (CFD) has been widely adopted to model the blood flow in coronary arteries [1-2]. The predicted WSS distribution can assist diagnosis and prognosis of arterial stenosis [3]. Besides the patient-specific anatomical geometry, proper boundary conditions plays an important role in the numerical results [4]. Due to the small lumen size of coronary artery, the acquisition of flow or pressure waveform proposes tremendous challenge, especially at the outlets of the coronary side branches. One prevailing method is to assign the outlet with the percentage of the total flow rate according to scale laws [5, 6]. This method is limited to the studies on normal arteries without stenosis, as the stenosis could lead to the change of flow rate distributions. Besides pressure boundary condition, more sophisticated methods are used to represent the downstream vasculature by flow-dependent formulation [7, 8]. This is based on the assumption that the flow resistance, compliance and impedance of the downstream vasculature are decided by its own anatomy rather than the upstream stenosis so that these parameters obtained from the normal model without stenosis can be applied to diseased models.

Although extensive simulations on coronary arteries have been conducted during the past decades, the studies on the effect of stenosis on the LAD arterial tree are limited. Shanmugavelayudam and colleagues [9] developed both 2D and 3D models of normal and diseased simplified LAD artery without side branch. Katritsis and colleagues [10] studied the LAD models with different degrees of stenosis to correlate vortices and flow recirculation with thrombus formation. Swillen and colleagues [2] only modelled the LAD with 75% and 90% stenosis, since their main purpose was to estimate the effect of LAD stenosis on the flow in left internal mammary artery (LIMA) to LAD bypass surgery. Kim and colleagues [11] simulated patient-specific coronary arteries with sophisticated boundary conditions. However, they mainly focused on the effect of stenosis on the flow rate in LAD. In this study, the porcine LAD models were studied under both pulsatile and steady flow conditions. The stenosis was imposed at the trunk of LAD tree between the first and second side branches, and then its effects on the total flow rate and the flow rate distribution were investigated. In addition, the WSS distributions for the models with different degrees of stenosis (0%, 25%, 50%, 75% and 90% area stenosis ratio) were analyzed.

II. MATERIALS AND METHODS

A normal porcine heart was prepared and scanned by computed tomography (CT) [1]. The LAD arteries were reconstructed from CT images as illustrated in Fig. 1. To

investigate the effects of stenosis, the trunk between side branch 1 (S1) and 2 (S2) was narrowed by 25%, 50%, 75% and 90% in area with respect to the host artery. All the imposed stenoses were concentric and had the same length.

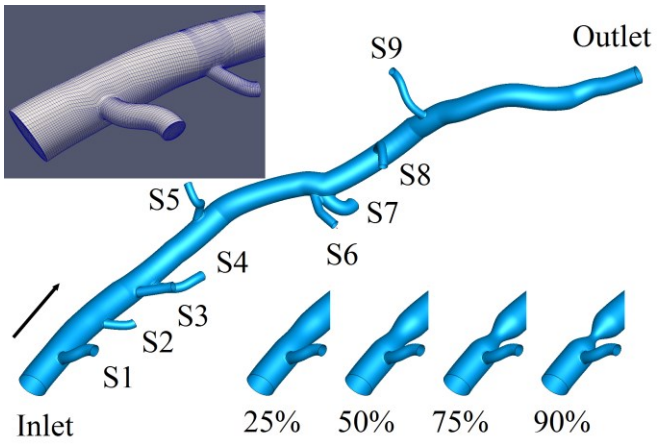

Figure 1. Reconstructed model of porcine LAD arterial tree with nine side branches and structured mesh. Note that the arrow indicates the flow direction.

The reconstructed CAD geometries were meshed with structured grids (Fig. 1) using grid generation software, ICEM (CFD 14.0). The same topology was applied to every model. Grid-independence was tested on the normal model under steady flow condition, with 4 sets of grids, viz. 5×10^5, 8×10^5, 11×10^5, and 1.4×10^6 cells respectively. A total of 8×10^5 elements were found to be sufficient, as the predicted WSS has less than 0.5% relative difference with the results predicted by 1.4×10^6 elements.

The 3D blood flow in the LAD is governed by the Navier-Stokes and continuity equations that can be written as:

$$\rho\left(\frac{\partial v}{\partial t}+v\cdot\nabla v\right)=\nabla\cdot\tau-\nabla P \quad (1)$$

$$\nabla\cdot v=0 \quad (2)$$

where ρ is the fluid density; v is the velocity vector; t is the time; P is the pressure; and τ is the stress tensor. The commercial CFD solver, FLUENT™ (Version 6.3.26), was adopted for the numerical simulation. The porcine blood was assumed to be Newtonian and incompressible with dynamic viscosity of 4 cP and density of 1,060 kg/m^3 [1].

The LAD models were assumed to be stationary and rigid with no slip boundary condition applied to the wall. The transient and time-averaged inlet velocity profiles (Fig. 2) were applied to the normal model for simulating the steady and unsteady flow respectively. In the normal LAD model, the percentage distribution of the total flow rate among the branches was first calculated according to the scaling law [6]. The obtained pressure waveform at the inlet was then used for simulating all the models (including those with stenosis) to investigate the effect of stenosis on the total flow rate.

Resistance boundary conditions were then applied to the outlets of all the models, which mean:

$$P^i_{outlet}=P^i_{back}+R^i\cdot Q^i_{outlet} \quad (3)$$

where P^i_{outlet} is the pressure at the outlet; R^i is the flow resistance, which is defined by the pressure and flow rate values of normal LAD model; Q^i_{outlet} is the flow rate; and P^i_{back} is the back pressure at i^{th} outlet. It was modelled by user defined function (UDF), which was compiled and loaded to the CFD solver. As a result, the downstream vasculatures were coupled to the LAD model, and the static pressure at each outlet was solved iteratively with an implicit algorithm.

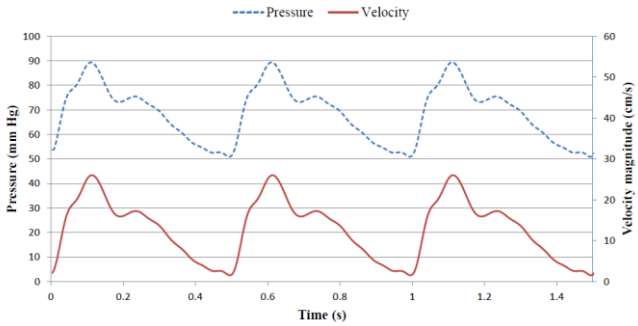

Figure 2. Temporal inlet velocity waveform (solid line) and resulted pressure waveform. (dashed line)

The convergence criterion was set as that the difference of the outlet pressure between two consecutive iterations was less than 1 Pa. After the time-step size independency test, the time-step size was set as 4ms. The unsteady-state simulations were performed over four cardiac cycles, and the results presented were extracted from the last cycle. The time-averaged WSS (TAWSS) over one cardiac cycle was calculated as:

$$TAWSS=\frac{1}{T}\int_0^T|\tau_w|dt \quad (4)$$

where τ_w is instantaneous wall shear stress vector and T is the duration of one cardiac cycle. The TAWSS distribution has the potential to identify atherosclerosis [2-4].

III. Results

Table 1 shows the flow rates and the distributions among side branches in normal and diseased models under both stead-state and unsteady-state. It can be found that the total flow rate and the distributions predicted by steady-state and unsteady-state simulations are similar to each other with the maximum discrepancy less than 1% and 0.5%, respectively. Comparing to the normal model, the model with 75% and 90% area stenosis has a total flow rate of 2.4% and 17.5% lower respectively. However, non-significant area stenosis (≤75%) only results in slight total flow rate reduction (≤0.5 ml/min) in contrast to the normal model. Instead of flow reduction, the flow rate through the first side branch (before the stenosis) increases due to the 'branch steal' [12]. The percentage of the outflow through the first branch increases from 13.2% of the normal model to 16.3% of the model with 90% area stenosis. The flow rate in the branches downstream of stenosis decreases. However, the effect of the stenosis diminishes at the downstream bifurcations, e.g. the flow rate percentage decreases from 9.8% to 9.5% at third bifurcation. The effect of stenosis vanishes at fifth bifurcation.

TABLE I. FLOW RATE AND PERCENTAGE OF TOTAL FLOW RATE DISTRIBUTIONS AMONG BRANCHES, IN NORMAL AND DISEASED MODELS PREDICTED USING STEADY-STATE AND UNSTEADY-STATE SIMULATIONS.

			Inlet	S1	S2	S3	S4	S5	S6	S7	S8	S9	Outlet
0%	Steady	ml/min	66.0	-8.6	-4.0	-5.2	-5.3	-3.3	-3.9	-10.7	-2.6	-2.0	-20.4
		%		13.0	6.1	7.9	8.0	5.0	5.9	16.2	4.0	3.0	30.9
	Unsteady	ml/min	65.4	-8.6	-4.0	-5.2	-5.2	-3.2	-3.9	-10.8	-2.6	-2.0	-20.0
		%		13.2	6.1	7.9	8.0	5.0	5.9	16.5	4.0	3.0	30.5
25%	Steady	ml/min	65.8	-8.6	-4.0	-5.2	-5.3	-3.3	-3.9	-10.7	-2.6	-2.0	-20.3
		%		13.1	6.1	7.9	8.0	5.0	5.9	16.2	4.0	3.0	30.8
	Unsteady	ml/min	65.1	-8.6	-4.0	-5.1	-5.2	-3.2	-3.8	-10.7	-2.6	-1.9	-19.9
		%		13.2	6.1	7.9	8.0	4.9	5.9	16.5	3.9	3.0	30.5
50%	Steady	ml/min	65.8	-8.60	-4.0	-5.2	-5.3	-3.3	-3.9	-10.7	-2.6	-2.0	-20.3
		%		13.1	6.0	7.9	8.0	5.0	5.9	16.2	4.0	3.0	30.8
	Unsteady	ml/min	64.9	-8.6	-4.0	-5.1	-5.2	-3.2	-3.8	-10.7	-2.6	-1.9	-19.8
		%		13.3	6.1	7.9	8.0	4.9	5.9	16.5	3.9	3.0	30.5
75%	Steady	ml/min	63.4	-8.7	-3.7	-5.0	-5.0	-3.1	-3.8	-10.2	-2.5	-1.9	-19.5
		%		13.7	5.9	7.8	7.9	5.0	5.9	16.2	4.0	3.0	30.7
	Unsteady	ml/min	63.8	-8.7	-3.8	-5.0	-5.1	-3.1	-3.8	-10.5	-2.5	-1.9	-19.4
		%		13.7	6.0	7.8	7.9	4.9	5.9	16.4	3.9	3.0	30.5
90%	Steady	ml/min	52.2	-8.7	-2.9	-3.9	-4.0	-2.5	-3.0	-8.2	-2.0	-1.5	-15.6
		%		16.6	5.6	7.4	7.6	4.8	5.8	15.7	3.9	2.9	29.9
	Unsteady	ml/min	53.7	-8.8	-3.1	-4.0	-4.1	-2.6	-3.1	-8.6	-2.1	-1.6	-16.0
		%		16.3	5.7	7.4	7.6	4.8	5.8	16.0	3.8	2.9	29.7

Fig. 3 shows the flow velocity magnitude contours on a sliced plane in the vicinity of the stenosis under the normal and diseased conditions with superimposed streamlines. It is worth noting that the flow fields obtained from the unsteady-state simulations are time-averaged. As anticipated, the stenosis accelerates the blood flow through its throat (Fig. 3). When the area stenosis is severe (≥75%), the jet flow through the throat impinges on the main trunk, and then redirected towards the myocardial side due to the curvature of the main trunk. In the wake of the severe stenosis, the flow near the myocardium (side branches) is dominated by the flow recirculation, which is initiated by the flow separation between the jet flow and the expanding throat. However, the flow recirculation opposite to the myocardium is weak due to the curvature of the trunk. Through the comparison between 75% and 90% area stenosis, it can be found that the region of flow recirculation (or vortex) increases with the degree of stenosis with its core located further downstream. In contrast, smooth flow is found for the model with non-significant stenosis (<75%). It can be found that the steady-state simulation results are similar to the time-averaged unsteady-state simulation results in terms of flow velocity magnitude and flow pattern.

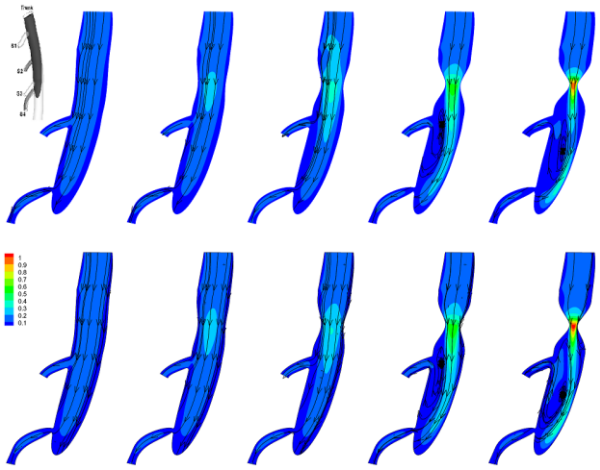

Figure 3. Velocity magnitude contours and streamlines: Time-averaged (upper) and steady (lower). Degree of stenosis increases from left to right, i.e. 0%, 25%, 50%, 75% and 90%.

Fig. 4 shows the WSS distributions on the normal and diseased models. Only the upper portion of the LAD coronary tree (from the entrance to the fifth side branch) is shown, because the influence of the stenosis on the lower portion is marginal even at 90% area stenosis. It can be found that the WSS distribution in the steady-state is similar to TAWSS distribution in the unsteady-state regardless of the degree of stenosis, though the former underestimated the maximum WSS with the highest discrepancy less than 10%. The maximum TAWSS in the normal condition is 12 Pa, and it increases to 79 Pa at 90% area stenosis. When the area stenosis is non-significant (<75%), the maximum TAWSS appears at the flow divider (near the ostium of side branch facing the blood flow in the trunk). TAWSS is elevated at the throat, where the velocity gradient increases as shown earlier in Fig. 3. Under the severe stenosis (≥75%), TAWSS near the throat exceeds those at flow dividers, and the jet flow escalates the TAWSS level on the curved LAD trunk opposite the third and fourth branches. Furthermore, low TAWSS region is observed on the main trunk opposite to the second side branch, where is in the wake of the stenosis, and it is consistent with the flow recirculation illustrated in Fig. 3.

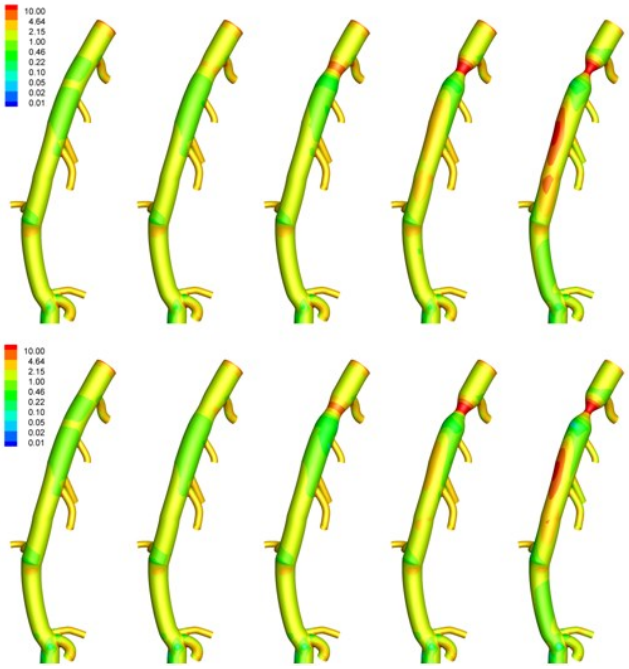

Figure 4. WSS distribution on the upper portion of LAD model: Time-averaged (upper) and steady (lower).

IV. DISCUSSION

The primary purpose of this work was to study the effects of stenosis on the flow rate, flow pattern and WSS distributions for LAD coronary tree using CFD method. The anatomical LAD model was reconstructed from the CT images of a health porcine heart. To estimate the effects of stenosis, four other LAD models with different degrees of concentric stenosis (25%, 50%, 75% and 90% area reduction) were introduced in the region between first and second side branches.

As anticipated, a lower degree of stenosis resulted in less flow rate reduction. Table 1 shows that only severe area stenosis ≥75% could result in an evident total flow rate reduction, which is consistent with other observations in LAD [2, 11], as the boundary conditions selected in this study were based on an anesthetized animal. The total flow rate reduction will be significant during exercising [7]. It is also found that the flow rate distribution among branches altered considerably at significant stenosis (≥75%). The effect of stenosis diminishes as the blood flows downstream.

Comparing to the unsteady-state simulation, the steady-state simulation results can fairly capture the dominant features in the aspects of total flow rate distribution, flow field in the vicinity of the stenosis and WSS [1].

In addition, it is believed that the high WSS initiate plaque rupture and the low WSS promotes atherosclerosis [4, 13, 14]. In this study, the TAWSS of the normal model is within 12 Pa, and the highest value is always observed at the flow divider, which is also demonstrated in other studies [1, 15].Therefore, stenosis may lead the atherosclerosis forming near the ostium of the closest downstream side branch initially. Only significant stenosis (≥75%) alters the TAWSS pattern dramatically. Due to the impingement of the jet flow through the throat onto the curved main trunk, the TAWSS level on the outer surface of the main trunk opposite to the third and fourth side branches escalated. In addition, the highest TAWSS appears at the throat instead of the flow divider. Simultaneously, a low TAWSS region is observed on the outer surface of the main trunk opposite to the second side branch, where flow recirculation occurs. As a result, atherosclerosis potentially develops in the wake of stenosis after the jet flow initiates the plaque rapture.

V. Conclusion

This study numerically analyzed the flow in porcine LAD arterial tree in the normal and diseased conditions with various degrees of stenosis. It has been demonstrated that the non-significant stenosis (<75%) does not affect the flow rate distribution among branches. For significant stenosis, the Myrrey's law is still valid for the branches far away from the stenosis. The steady-state simulation is capable of preserve the dominant flow feature in the aspects of flow field and WSS, when comparing with the unsteady-state simulation. This study has demonstrated that the stenosis may promote atherosclerosis near the ostium of the closest downstream side branch initially. For significant stenosis, the potential atherosclerosis site might relocate to the wake of the stenosis, where flow recirculation occurs.

Acknowledgment

This research is supported by the National Research Foundation, Singapore under its Cooperative Basic Research Grant and administered by the Singapore Ministry of Health's National Medical Research Council (NMRC/EDG/1037/2011). The support of SingHealth Foundation Research Grant (SHF/FG503P/2012) is gratefully acknowledged.

References

[1] Y. Huo, T. Wischgoll and G. S. Kassab, "Flow patterns in three-dimensional porcine epicardial coronary arterial tree," *American Journal of Physiology. Heart and Circulatory Physiology*, vol. 293, pp. H2959–70, 2007.

[2] A. Swillens, D. M. Witte, H. Nordgaard, L. Løvstakken, V. D. Loo, B. Trachet, J. Vierendeels and P. Segers, "Effect of the degree of LAD stenosis on "competitive flow" and flow field characteristics in LIMA-to-LAD bypass surgery," *Medical & Biological Engineering & Computing*, vol. 50, pp. 839–49, 2012.

[3] F. Rikhtegar, J. A. Knight, U. Olgac, S. C. Saur, D. Poulikakos, W. Marshall, P. C. Cattin, H. Alkadhi and V. Kurtcuoglu, "Choosing the optimal wall shear parameter for the prediction of plaque location-A patient-specific computational study in human left coronary arteries," *Atherosclerosis*, vol. 221, pp. 432–7, 2012.

[4] D. Gallo, D. G. Santis, F. Negri, D. Tresoldi, R. Ponzini, D. Massai, M. A. Deriu, P. Segers, B. Verhegghe, G. Rizzo and U. Morbiducci, "On the use of in vivo measured flow rates as boundary conditions for image-based hemodynamic models of the human aorta: implications for indicators of abnormal flow," *Annals of Biomedical Engineering*, vol. 40, pp. 729–41, 2012.

[5] B. C. D. Murray, "The Physiological principle of minimum work. I.," *Proceedings of the National Academy of Sciences of the United States of America*, vol. 12, pp. 207–214, 1926.

[6] G. S. Kassab, "Scaling laws of vascular trees: of form and function," *American Journal of Physiology. Heart and Circulatory Physiology*, vol. 290, pp. H894–903, 2006.

[7] H. J. Kim, I. E. Vignon-Clementel, C. A. Figueroa, J. F. LaDisa, K. E. Jansen, J. A. Feinstein and C. A. Taylor, "On coupling a lumped parameter heart model and a three-dimensional finite element aorta model," *Annals of Biomedical Engineering*, vol. 37, pp. 2153–69, 2009.

[8] A. C. Benim, A. Nahavandi, A. Assmann, D. Schubert, P. Feindt and S. H. Suh, "Simulation of blood flow in human aorta with emphasis on outlet boundary conditions," *Applied Mathematical Modelling*, vol. 35, pp. 3175–3188, 2011.

[9] S. K. Shanmugavelayudam, D. A. Rubenstein and W. Yin, "Effect of geometrical assumptions on numerical modeling of coronary blood flow under normal and disease conditions," *Journal of Biomechanical Engineering*, vol. 132, pp. 061004, 2010.

[10] D. G. Katritsis, A. Theodorakakos, I. Pantos, A. Andriotis, E. P. Efstathopoulos, G. Siontis, N. Karcanias, S. Redwood and M. Gavaises, "Vortex formation and recirculation zones in left anterior descending artery stenoses: computational fluid dynamics analysis," *Physics in Medicine and Biology*, vol. 55, pp. 1395–411, 2010.

[11] H. J. Kim, I. E. Vignon-Clementel, J. S. Coogan, C. A. Figueroa, K. E. Jansen and C. A. Taylor, "Patient-specific modeling of blood flow and pressure in human coronary arteries," *Annals of Biomedical Engineering*, vol. 38, pp. 3195–3209, 2010.

[12] K. L. Gould, R. Kirkeeide and N. P. Johnson, "Coronary branch steal experimental validation and clinical implications of interacting stenosis in branching coronary arteries," *Circ Cardiovasc Imaging*, vol. 3, pp. 701-709, 2010.

[13] K. Perktold, M. Hofer, G. Rappitsch, M. Loew, B. D. Kuban and M. H. Friedman, "Validated computation of physiologic flow in a realistic coronary artery branch," *Journal of Biomechanics*, vol. 31, pp. 217–28, 1998.

[14] H. C. Groen, L. Simons, V. d. Q. J. A. Bouwhuijsen, E. M. H. Bosboom, F. J. H. Gijsen, V. d. A. G. Giessen, V. d. F. N. Vosse, A. Hofman, V. d. A. F. W. Steen, J. C. M. Witteman, V. d. A. Lugt and J. J. Wentzel, "MRI-based quantification of outflow boundary conditions for computational fluid dynamics of stenosed human carotid arteries," *Journal of Biomechanics*, vol. 43, pp. 2332–8, 2010.

[15] J. V. Soulis, T. M. Farmakis, G. D. Giannoglou and G. E. Louridas, " Wall shear stress in normal left coronary artery tree," *Journal of Biomechanics*, vol. 39, pp. 742–9, 2006.